Communications in Physics, Vol. 35, No. 3 (2025), pp. 203-214

DOI: https://doi.org/10.15625/0868-3166/22722

Thermodynamic properties of the first-order magnetic transition in the highly anisotropic 2D Blume-Capel model

Phong H. Nguyen, and Giang H. Bach[†]

Faculty of Physics, University of Science, Vietnam National University, Hanoi, 334 Nguyen Trai Street, Thanh Xuan, Hanoi, Vietnam

E-mail: †gbach@hus.edu.vn

Received 17 April 2025 Accepted for publication 2 July 2025 Published 24 September 2025

Abstract. The effect of anisotropy on the first-order magnetic transition (FOMT) in the highly anisotropic systems, such as perovskite manganite oxides, is investigated using Monte Carlo simulations of a two-dimensional (2D) spin S=1 Blume-Capel model with random anisotropy. For sufficiently large values of anisotropy probability p and corresponding amplitude p, the second-order magnetic transition (SOMT) transforms into the FOMT. The presence of the FOMT is indicated not only by a sharp discontinuity in the magnetic moment at the critical temperature $T_C^{(1)}$, but also by significant changes in the internal energy and magnetic moment histograms. As the type of the phase transition changes, thermodynamic observables display distinctly different behavior around $T_C^{(1)}$. A phase diagram illustrating the SOMT-to-FOMT crossover induced by random anisotropy in high-p regimes is successfully constructed.

Keywords: Blume-Capel model; random anisotropy; Monte Carlo simulation, first-order magnetic transition.

Classification numbers: 75.40.Mg; 75.30.Gw; 75.30.-m.

1. Introduction

The magnetocaloric effect (MCE) has attracted considerable research interest for its potential to revolutionize heating and cooling technologies [1–3]. Materials that undergo a sharp decline in magnetic moment at the Curie temperature, characteristic of a first-order magnetic transition (FOMT), are particularly promising for achieving a giant MCE [3–11]. Notably, several perovskite manganite oxides, $AMnO_3$, doped at both the A and B sites of ABO_3 , exhibit FOMT and display significant changes in magnetic entropy under an external magnetic field, a hallmark

of giant MCE [3, 12–17]. In these materials, the nature of the phase transition, whether it is a continuous second-order magnetic transition (SOMT) or a discontinuous FOMT, is thought to be influenced by single-ion magnetic anisotropy. This anisotropy arises from the random distribution of multi-valent Mn ions and their associated magnetic moments [12–20].

The spin S = 1 Blume-Capel (BC) model is widely recognized as a fundamental theoretical framework for studying FOMT induced by random anisotropy [21–23]. Within this model, our recent work employing advanced Monte Carlo techniques successfully established a phase diagram that illustrates how random anisotropy influences the nature of the phase transition. Unlike effective field theory (EFT), which struggles with the presence of multiple local minima in the free energy landscape [24], Monte Carlo methods are capable of overcoming this limitation. They also provide two key indicators for identifying the transition type: the characteristic behavior of the magnetic moment, and the distinct distribution patterns observed in the internal energy and magnetic moment histograms. Building on the strengths of these methods, we continue to apply them to explore the magnetic properties of perovskite manganite oxides under the influence of random anisotropy.

In general, as observed in the perovskite manganite oxides mentioned above [3, 12–17], FOMT occurs only at very low dopant concentrations, corresponding to highly anisotropic systems. In our recent work [25], we examined the influence of random anisotropy on FOMT and the associated MCE for specific cases, without focusing on how variations in anisotropy amplitude affect thermodynamic quantities. In this study, we specifically investigate thermodynamic behaviors, including magnetic moment, internal energy, specific heat, and spin susceptibility, highlighting their distinct responses to phase-transition type changes induced by different anisotropy amplitudes in regimes of high anisotropy probability. Additionally, to confirm the phase-transition type change and the position of the tri-critical point, we analyze internal energy and magnetic moment histograms for both FOMT and SOMT. Based on the behavior of these thermodynamic quantities around the phase-transition temperatures, we also construct a phase diagram in the $T_C - D$ plane, illustrating the relationship between the critical temperature, anisotropy amplitude, and phase-transition type.

The structure of this paper is as follows: Sec. 2 provides a concise overview of the model and the computational approach. Sec. 3 delves into the Monte Carlo data analysis and presents the results. Finally, Sec. 4 presents our conclusions.

2. Model and computational method

We consider a square spin-lattice of $N = L \times L$ sites, where each site has q = 4 nearest neighbors, governed by the Blume-Capel model with random anisotropy (Fig. 1). The system is subject to periodic boundary conditions in both directions and is defined by the following Hamiltonian:

$$H_{BC} = -J \sum_{\langle i,j \rangle} S_i^z S_j^z + \sum_j D_j (S_j^z)^2, \tag{1}$$

where the variable S_i^z assuming values of ± 1 or 0, corresponds to the z-component of a classical spin S=1 at site i. The first summation runs over all nearest-neighbor pairs $\langle i,j\rangle$, where the exchange coupling J>0 promotes ferromagnetic interactions. The random anisotropic field D_j , varying by site, follows a bimodal distribution [6, 25–28],

$$P(D_i) = p\delta(D_i - D) + (1 - p)\delta(D_i). \tag{2}$$

Here, the site-dependent anisotropic field adopts the value D with probability p or vanishes with probability 1-p. In the subsequent part, a unit system is employed in which the physical quantities D, internal energy E, and temperature T are expressed in a dimensionless form with units defined by J=1 and where the Boltzmann constant is taken as $k_B=1$. For example, the temperature τ , measured in Kelvin, is converted into its dimensionless form as $T=k_B\tau/J$.

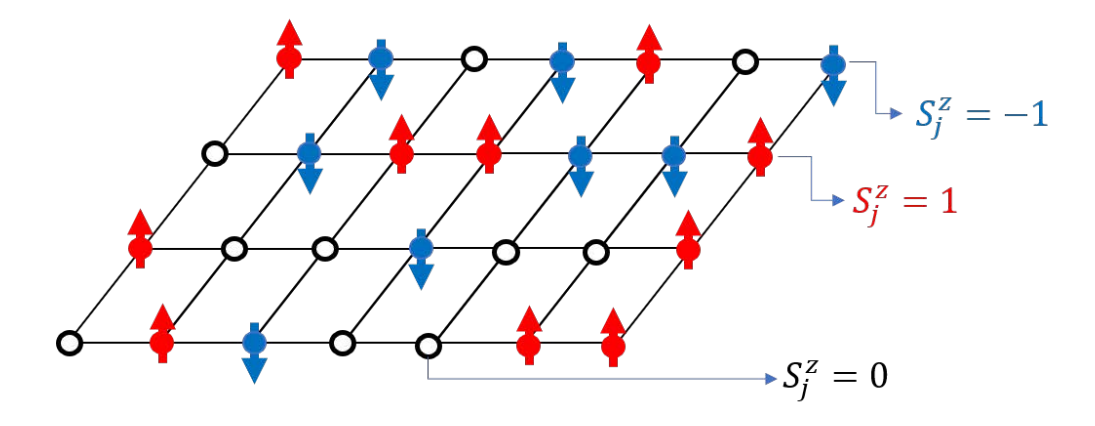


Fig. 1. Schematic representation of the square spin lattice in the Blume-Capel model.

The cluster hybrid algorithm [29], which combines the Metropolis algorithm [30] and the Wolff algorithm [31], is utilized to update the spin configuration. By integrating the Wolff cluster-flipping process, this method mitigates the problem of critical slowing down while also facilitating transitions between spin states of varying magnitudes through the Metropolis algorithm.

Linear system sizes of L=16,32,64,128, and 200 are considered in this study. The system is first equilibrated with the heat bath over 10^5 iterations, followed by 3×10^5 additional iterations to determine the average of the thermodynamic quantities. Each iteration comprises one Metropolis sweep along with approximately r ($r\sim5$) Wolff steps.

Moreover, in order to enhance the efficiency of reaching stable thermal equilibrium and assist the system in escaping local minima near the transition temperature, the parallel tempering or replica exchange method [32] is applied. This technique improves the system's capacity to tunnel through entropic barriers by transferring fluctuations from higher-temperature states to lower-temperature ones. As a result, the system's behavior and transition temperatures can be analyzed with greater accuracy.

Once the cluster hybrid algorithm determines the estimated transition temperature T_C , we arrange a set of $N_T = 40$ temperatures, labeled as T_i , symmetrically around T_C . These N_T temperature replicas are simulated concurrently, with 10^5 swap attempts proposed during the process. The exchange of neighboring replica configurations occurs if the swap acceptance criterion, defined as $P(\beta_i \Leftrightarrow \beta_{i+1}) = \min\{1, \exp(\Delta\beta \Delta E)\}$, is fulfilled. In this expression, $\Delta\beta = \beta_{i+1} - \beta_i$ represents the difference between adjacent inverse temperatures, $\beta_i = 1/T_i$, while $\Delta E = E_{i+1} - E_i$ corresponds to the variation in internal energy. To determine the average thermodynamic quantities, 100 Monte Carlo steps are executed between successive swaps. The thermodynamic quantities evaluated include [33]:

Total internal energy per spin,

$$E = \frac{\langle H \rangle}{N},\tag{3}$$

Magnetic moment per spin,

$$m = \frac{\langle \sum_{i=1}^{N} S_i^z \rangle}{N},\tag{4}$$

Magnetic susceptibility per spin,

$$\chi = \frac{1}{N^2} \frac{\langle (\sum_{i=1}^N S_i^z)^2 \rangle - \langle \sum_{i=1}^N S_i^z \rangle^2}{T},\tag{5}$$

Specific heat,

$$C_V = \frac{1}{N^2} \frac{\langle H^2 \rangle - \langle H \rangle^2}{T^2}.$$
 (6)

To verify the correct physical behavior of the system, both configurational and statistical averages of the aforementioned quantities are evaluated. For each temperature and system size, a minimum of k = 10 configurational samples is generated. Consequently, each thermodynamic quantity O is computed accordingly,

$$[\langle O \rangle] = \frac{1}{k} \sum_{i=1}^{k} \langle O \rangle_i. \tag{7}$$

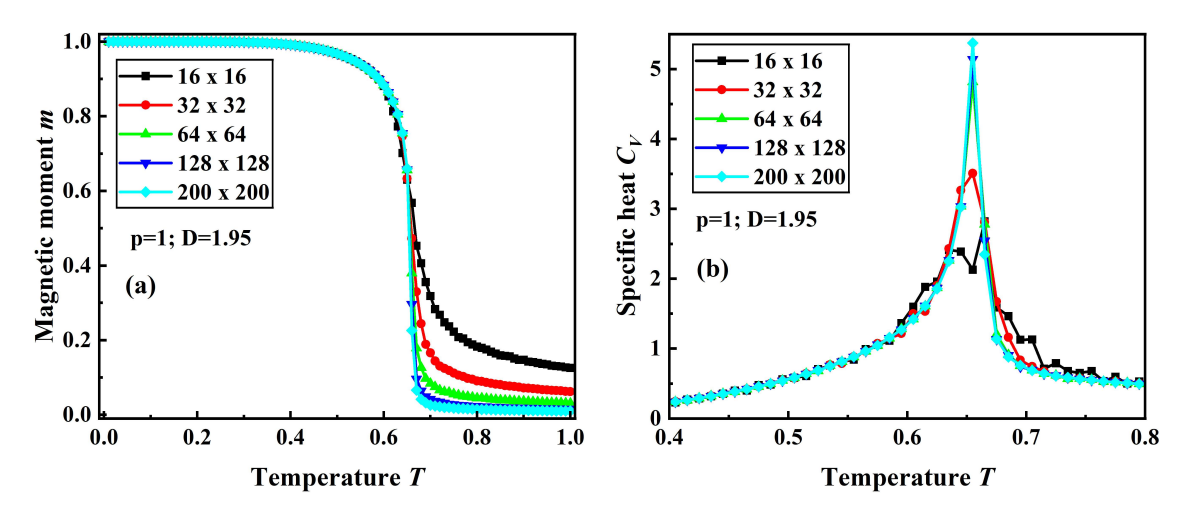


Fig. 2. (Color online) Temperature dependence of (a) the magnetic moment and (b) the specific heat for various system sizes. The parameters are set to p = 1 and D = 1.95.

Since finite-size effects in phase transition studies cannot be overlooked, it is necessary to evaluate the reliability of simulations by modifying the system size $N = L \times L$, as illustrated in Fig. 2. For small system sizes, such as $N = 16 \times 16$ and $N = 32 \times 32$, a nonzero magnetic moment is observed beyond the critical temperature, accompanied by a considerable shift in the specific heat peak as the lattice size changes. This shift distinctly reflects finite-size effects in statistical physics, since the system's behavior deviates from the thermodynamic limit, where critical phenomena are well-defined [34, 35]. For large system sizes, such as $N = 128 \times 128$ and

 $N = 200 \times 200$, no significant changes in magnetic moment behavior or the specific heat peak position are caused by further lattice expansion. To maintain a balance between computational efficiency and accuracy, simulations are subsequently performed with a lattice size of $N = 128 \times 128$, ensuring sufficient precision in determining physical properties and the critical temperature.

3. Results and discussion

Because we are primarily interested in the FOMT occurring in highly anisotropic systems, we restrict our calculations to two values of the anisotropy probability: p = 1 and p = 0.9, with $D \le 2.2$. The case p = 1 corresponds to an anisotropic system without disorder, whereas disorder is introduced in the p = 0.9 case. In this study, we do not consider the scenario p = 0.8, as it has been thoroughly investigated in our previous work [25].

3.1. Case 1: FOMT without disorder (p = 1)

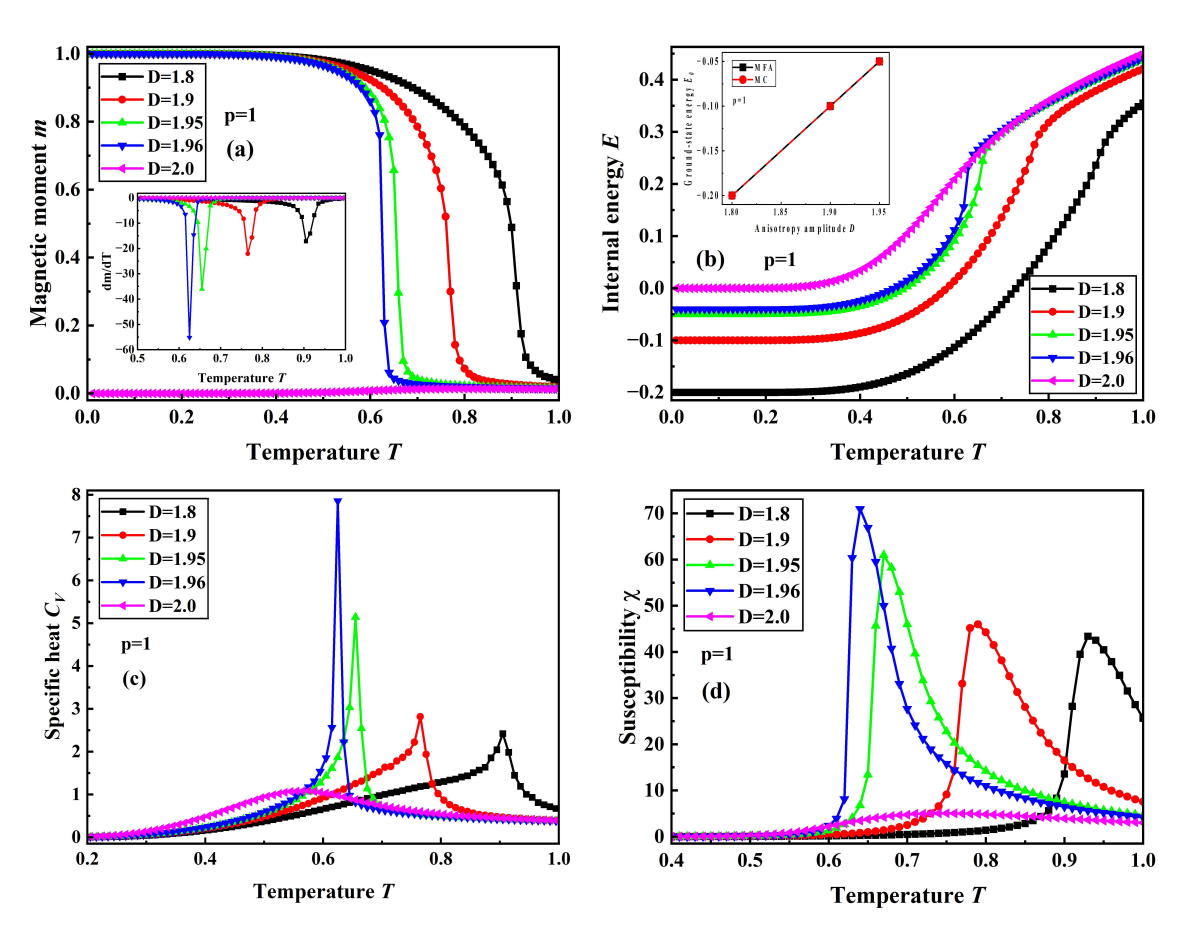


Fig. 3. (Color online) Thermodynamic quantities as functions of temperature for different values of D at p=1: (a) magnetic moment, (b) internal energy, (c) specific heat, and (d) magnetic susceptibility. The inset in panel (a) displays the derivative dm/dT associated with the main curves.

First, we consider the original Blume-Capel model without disorder (p=1), in which the FOMT arises solely due to a sufficiently large anisotropy amplitude D, without requiring any randomness. The temperature dependence of thermodynamic quantities, including (a) magnetic moment, (b) internal energy, (c) specific heat, and (d) magnetic susceptibility for this case (p=1) with various values of the anisotropy parameter (D=1.8, 1.9, 1.95, 1.96, 2.0) is shown in Fig. 3.

We begin by examining Fig. 3(a), which displays the temperature dependence of the magnetic moment. For a high anisotropy amplitude $D=2.0=\frac{qJ}{2p}$, which is the limit discussed in our previous work [25], the magnetic moment vanishes (m=0) across all temperatures, indicating the absence of a phase transition. This behavior can be attributed to the fact that when the anisotropy energy exceeds the exchange interaction $(pD \ge \frac{qJ}{2})$, the system energetically favors the non-magnetic transverse spin state $S^z=0$, even at low temperatures.

When the anisotropy parameter is slightly reduced to the range $1.95 \le D < 2.0$, the FOMT is observed. This transition is characterized by a steep fall in the magnetic moment from a finite value to zero at the critical temperature $T_C^{(1)}$, which corresponds to the Curie temperature of the FOMT. For D=1.95, this pronounced change occurs at $T_C^{(1)}=0.66$, as indicated by a sharp downward spike in the temperature derivative of the magnetic moment, dm/dT, shown in the inset of Fig. 3(a). As the anisotropy magnitude D is further reduced below 1.95, the sharp drop in the magnetic moment becomes increasingly diffuse. This behavior reflects a shift from FOMT to SOMT, accompanied by a rise in the critical temperature $T_C^{(2)}$ as D decreases from 1.9 to 1.8.

SOMT, accompanied by a rise in the critical temperature $T_C^{(2)}$ as D decreases from 1.9 to 1.8. In the regime $D < \frac{qJ}{2p}$, where a phase transition occurs, the ground state $(T \approx 0)$ exhibits a fully saturated magnetic moment (m=1). This behavior arises because, in the absence of thermal fluctuations, the exchange interaction dominates the anisotropy energy, causing all spins to align parallel in the $|S^z|=1$ state. Based on this reasoning, we employ a mean-field approximation (MFA) to estimate the ground state energy:

$$E_0 = -\frac{qJ}{2} + pD. \tag{8}$$

These MFA results are identical to those obtained from Monte Carlo simulations, as shown in the inset of Fig. 3(b), where the ground-state energy E_0 exhibits a linear dependence on D for a fixed value of p.

The FOMT-to-SOMT transition is evident not only in the magnetic moment but also in the behavior of the internal energy, specific heat, and spin susceptibility, as shown in Fig. 3(b),(c),(d), where the peaks of specific heat and spin susceptibility occur at the corresponding critical temperatures. For D=2.0, the internal energy changes smoothly with temperature, making it difficult to determine whether a phase transition is present. In addition, the peaks in the specific heat and spin susceptibility are broad and shallow, suggesting that they are resulted from finite-size effects rather than from a true phase transition in the thermodynamic limit. This is consistent with the behavior of the magnetic moment, which remains zero for all temperatures.

At D=1.95, the internal energy shows a more rapid change at $T_C^{(1)}$, accompanied by significantly higher and sharper peaks in the specific heat and spin susceptibility compared to those at lower anisotropy values. These features provide strong evidence for the occurrence of the FOMT. As D decreases further to values such as 1.9 and 1.8, the temperature dependence of the internal energy at $T_C^{(2)}$ becomes smoother. Meanwhile, the peaks in specific heat and spin susceptibility

become broader and lower, reflecting a weakening of the transition and signaling the presence of the SOMT.

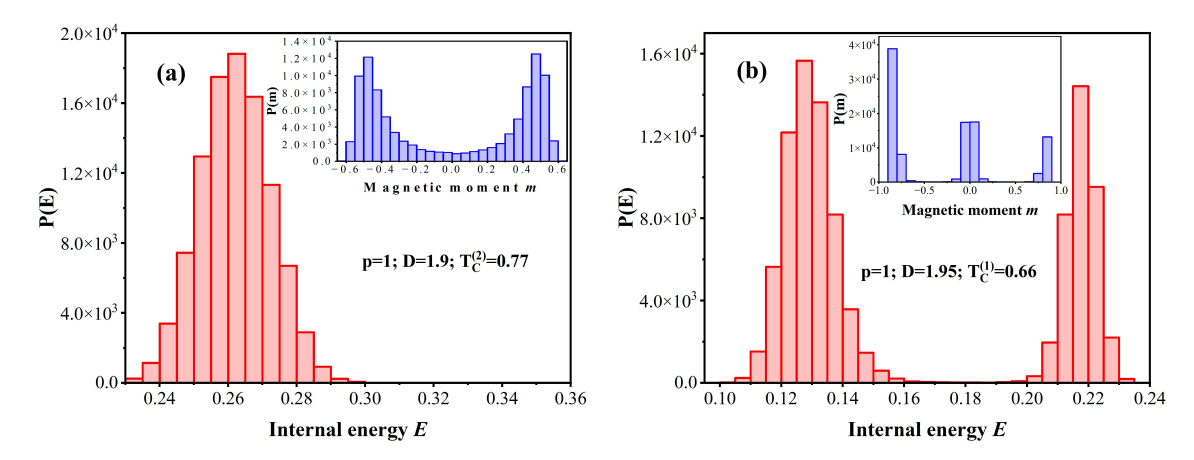


Fig. 4. Histogram of energy and magnetic moment (inset) with p = 1, D = 1.9, $T_C^{(2)} = 0.77$ (a); p = 1, D = 1.95, $T_C^{(1)} = 0.66$ (b).

To differentiate FOMT from SOMT, we display the histograms of the internal energy P(E) and the magnetic moment P(m), which clearly reveal the presence of FOMT or SOMT. A Gaussian-like shape in P(E) together with a symmetric double-peak structure in P(m), corresponding to a single dominant ferromagnetic state, signals the SOMT. This behavior is observed in Fig. 4(a) for p=1, D=1.9 at the critical temperature $T_C^{(2)}=0.77$. When the anisotropy increases to D=1.95, the single-peak form of P(E) evolves into a distinct double-peak structure, as shown in Fig. 4(b), indicating two preferred configurations: one with zero magnetic moment (paramagnetic) and the other with a finite value of magnetic moment (ferromagnetic). This is further reinforced by the three-peak pattern in P(m) (see the inset). These characteristics of P(E) and P(m) at $T_C^{(1)}=0.66$ strongly support the FOMT.

3.2. Case 2: FOMT with disorder (p = 0.9)

In the second case, we investigate the effect of disorder on the FOMT in regimes of high anisotropy probability, specifically for p=0.9. This effect becomes apparent when examining how (a) magnetic moment, (b) internal energy, (c) specific heat, and (d) spin susceptibility evolve with temperature across different anisotropy strengths ($D=1.8,\,1.9,\,2.0,\,2.1,\,2.15,\,2.16,\,2.2$), as shown in Fig. 5. As the anisotropy amplitude varies, the qualitative behavior of the thermodynamic quantities in Fig. 5 mirrors that observed in other FOMTs presented in Fig. 3.

For $D = 2.2 \approx \frac{qJ}{2p}$, no phase transition is observed. This is reflected in the vanishing magnetic moment, specific heat, and spin susceptibility at all temperatures, as shown in Fig. 5(a), (c), and (d), respectively. Consistent with the behavior of these thermodynamic quantities, the internal energy in Fig. 5(b) follows an almost linear trend, showing no indication of a critical temperature.

A slight reduction of D from 2.2 induces the FOMT within the range of $2.15 \le D < 2.2$. At D = 2.15, Fig. 5(a) reveals a sharp discontinuity in the magnetic moment, which abruptly drops from a nearly saturated value $m \approx 1$ to zero at the Curie temperature $T_C^{(1)} = 0.47$. This transition

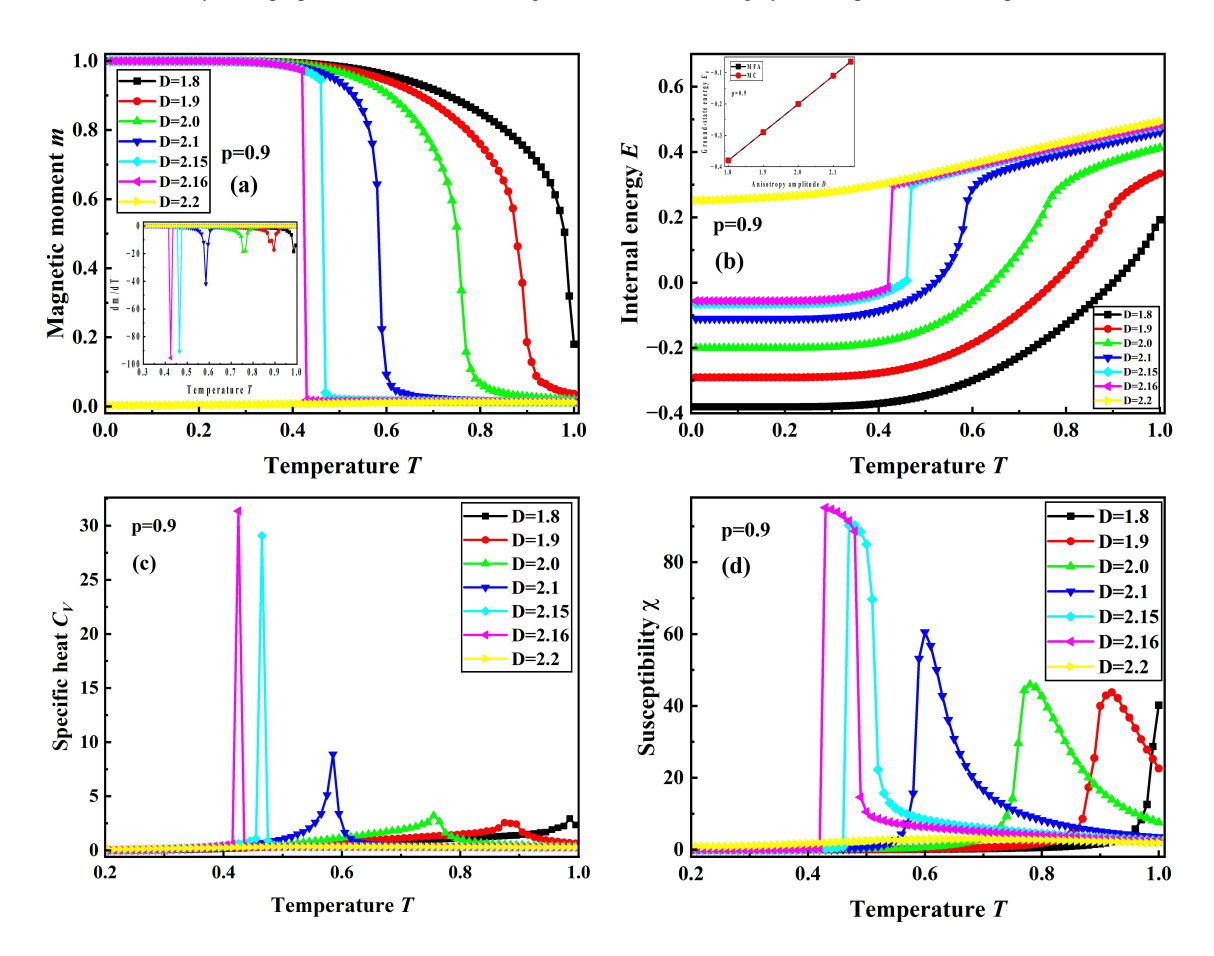


Fig. 5. (Color online) Thermodynamic quantities as functions of temperature for different values of D at p=0.9: (a) magnetic moment, (b) internal energy, (c) specific heat, and (d) magnetic susceptibility. The inset in panel (a) displays the derivative dm/dT associated with the main curves.

is accompanied by a deep inverse peak in the derivative of the magnetic moment to temperature dm/dT, as seen in the inset of Fig. 5(a). In line with this behavior, both the specific heat and spin susceptibility show sharp, high peaks that are more pronounced than those at lower D, while the internal energy in Fig. 5(b) exhibits a sudden jump, indicating the latent heat associated with the first-order nature of the transition at $T_C^{(1)}$.

For D < 2.15 at p = 0.9, the system instead undergoes the SOMT. As D decreases, the

For D < 2.15 at p = 0.9, the system instead undergoes the SOMT. As D decreases, the magnetic moment no longer shows a sharp drop but rather a gradual decline, replacing the discontinuity seen in the FOMT. Correspondingly, both the specific heat and spin susceptibility exhibit much weaker and narrower peaks, and the internal energy increases smoothly around the transition temperature $T_C^{(2)}$.

Regarding the ground state, the MFA results given by Eq.(8) are in complete agreement with the Monte Carlo results, as shown in the inset of Fig. 5(b). Both approaches reveal a linear dependence of the ground-state energy E_0 on D for a fixed value of p.

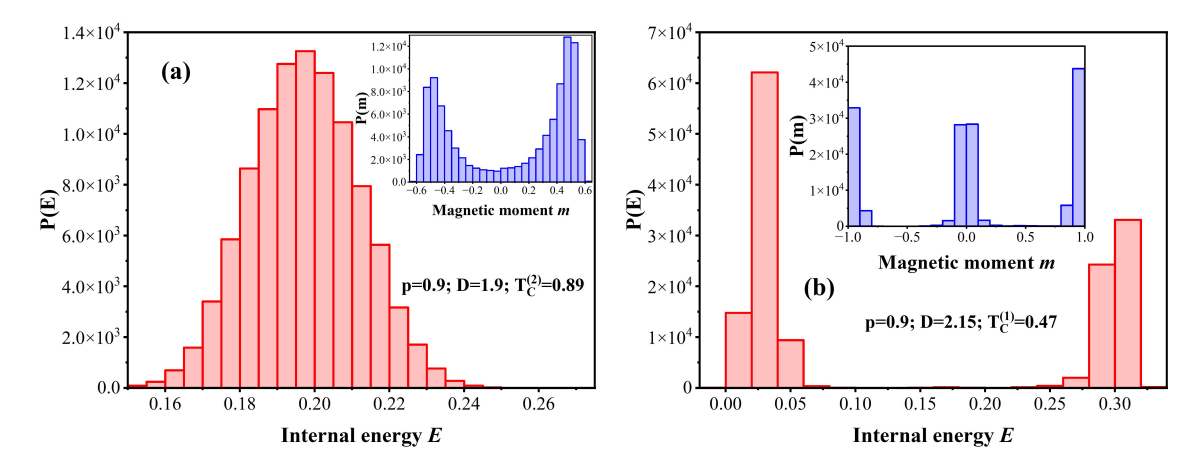


Fig. 6. Histogram of energy and magnetic moment (inset) with p = 0.9, D = 1.9, $T_C^{(2)} = 0.89$ (a); p = 0.9, D = 2.15, $T_C^{(1)} = 0.47$ (b).

As shown in Fig. 6, and qualitatively similar to the results in Fig. 4, two distinct types of distributions in the internal energy and magnetic moment histograms are observed, corresponding to the SOMT and FOMT. For p=0.9 and D=1.9, Fig. 6(a) illustrates the SOMT at the critical temperature $T_C^{(2)}=0.89$, characterized by a Gaussian-like P(E) and a symmetric double peak in P(m). These two peaks in P(m) indicate that the system favors a single ferromagnetic state, with fluctuations between equivalent magnetic moment directions. In contrast, Fig. 6(b) presents the FOMT at D=2.15, identified by a double-peak structure in P(E) at $T_C^{(1)}=0.47$, replacing the single-peak form seen in the SOMT. This is accompanied by a triple-peak structure in P(m), suggesting coexistence between two distinct configurations: a nearly saturated ferromagnetic state and a paramagnetic state with zero magnetic moment.

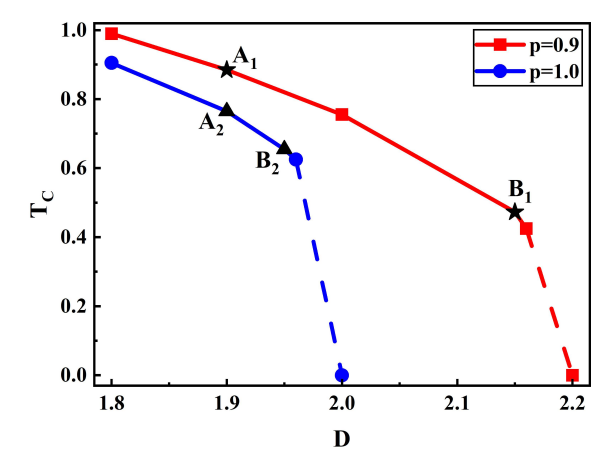


Fig. 7. Phase diagram showing the dependence of the critical temperature on the anisotropic factor for p = 1 and p = 0.9.

The mechanism behind the FOMT can be outlined as follows: when $p \geq 0.7$ and $pD \lesssim \frac{qJ}{2}$, the system tends to occupy the low-energy spin state with $|S^z|=1$ at temperatures below the Curie point, resulting in a ferromagnetic (FM) phase characterized by a finite magnetic moment. As the temperature increases and approaches the Curie temperature $T_C^{(1)}$, the majority of spins shift from the $|S^z|=1$ state to the nearby excited state $S^z=0$. This rapid change leads to a sudden collapse of the magnetic moment, indicating a first-order magnetic transition.

The behaviors of the thermodynamic observables for p=0.9 and p=1 are summarized in the phase diagram shown in Fig. 7. This diagram illustrates how the critical temperature T_C varies with the anisotropy strength D, where SOMT and FOMT are indicated by solid and dotted lines, respectively, for each value of p. The star labeled A_1 and the triangle labeled A_2 mark the SOMT critical temperatures $T_C^{(2)}$, with corresponding internal energy and magnetic moment histograms shown in Fig. 4(a) and Fig. 6(a). Likewise, the star labeled B_1 and the triangle labeled B_2 denote the FOMT critical temperatures $T_C^{(1)}$, with related histograms presented in Fig. 4(b) and Fig. 6(b). In both cases, the SOMT and FOMT lines meet at points B_1 and B_2 for p=0.9 and p=1, respectively, identifying these as the tri-critical points for each probability.

4. Conclusions

Using Monte Carlo simulations, we have studied the influence of anisotropy on the first-order magnetic transition (FOMT) in highly anisotropic systems, such as perovskite manganite oxides, within the framework of the two-dimensional spin S=1 Blume-Capel model with random anisotropy. For sufficiently high anisotropy probability p, adjusting the anisotropy amplitude D causes the system to exhibit a transformation from the second-order magnetic transition (SOMT) to the FOMT, as shown in the phase diagram plotted in the critical temperature versus anisotropy magnitude (T_C-D) plane. This diagram highlights the tri-critical points where the SOMT and FOMT lines intersect, located at D=2.15, $T_C^{(1)}=0.47$ for p=0.9, and at D=1.95, $T_C^{(1)}=0.66$ for p=1.

When the conditions $p \ge 0.7$ and $pD \lesssim \frac{qJ}{2}$ are met, the system exhibits a FOMT, characterized by distinct features in the thermodynamic quantities at the critical temperature $T_C^{(1)}$. Specifically, a double-peak appears in the internal energy histogram P(E), along with a triple-peak structure in the magnetic moment histogram P(m). The magnetic moment m shows a sharp drop, accompanied by a deep inverse peak in its temperature derivative dm/dT. Additionally, the internal energy E undergoes a sudden jump. Finally, remarkable high and narrow peaks are observed in both the specific heat C_V and the magnetic susceptibility χ .

Acknowledgements

This research was funded by the VNU University of Science, grant number TN.24.05.

Authors contributions

Phong H. Nguyen: Writing – Review - Editing, Resources, Methodology, Investigation, Validation, Visualization, Data Curation, Funding Acquisition. **Giang H. Bach**: Validation, Visualization, Editing, Formal Analysis, Supervision.

Conflict of interest

The authors have no conflict of interest to declare.

References

- [1] S. Kumar, G. G. Riera, A. Arauzo, J. Hruby, S. Hill, L. Bogani et al., On-surface magnetocaloric effect for a van der waals gd 2d mof grown on si, J. Mater. Chem. A 12 (2024) 6269.
- [2] X.-Q. Zheng and B.-G. Shen, The magnetic properties and magnetocaloric effects in binary r–t (r = pr, gd, tb, dy, ho, er, tm; t = ga, ni, co, cu) intermetallic compounds, Chin. Phys. B **26** (2017) 027501.
- [3] F. Guillou, A. K. Pathak, D. Paudyal, Y. Mudryk, F. Wilhelm, A. Rogalev et al., Non-hysteretic first-order phase transition with large latent heat and giant low-field magnetocaloric effect, Nat. Commun. 9 (2018) 2925.
- [4] F. Guillou, G. Porcari, H. Yibole, N. van Dijk and E. Bruck, *Taming the first-order transition in giant magne-tocaloric materials*, Adv. Mater. **26** (2014) 2671.
- [5] L. Li, Y. Yuan, Y. Zhang, T. Namiki, K. Nishimura, R. Pottgen et al., Giant low field magnetocaloric effect and field-induced metamagnetic transition in tmzn, Appl. Phys. Lett. 107 (2015) 132401.
- [6] G. H. Bach, O. K. T. Nguyen, C. V. Nguyen and C. T. Bach, First order magnetization process in polycrystalline perovskite manganite, Mater. Trans. 56 (2015) 1320.
- [7] A. Biswas, N. A. Zarkevich, A. K. Pathak, O. Dolotko, I. Z. Hlova, A. V. Smirnov et al., First-order magnetic phase transition in pr2in with negligible thermomagnetic hysteresis, Phys. Rev. B 101 (2020) 224402.
- [8] S. Ghosh, T. Paramanik and I. Das, Magnetic phase transitions in r5pd2 (r = ho, dy, dy0.6gd0.4) compounds, J. Supercond. Nov. Magn. 37 (2024) 231.
- [9] D. Guo, L. M. Moreno-Ramirez, C. Romero-Muniz, Y. Zhang, J.-Y. Law, V. Franco et al., First- and second-order phase transitions in re6co2ga (re = ho, dy or gd) cryogenic magnetocaloric materials, Sci. China Mater. 64 (2021) 2846
- [10] L. Xi, X. Zheng, Y. Gao, J. Xu, C. Liu, D. Wang et al., Giant low-field magnetocaloric effect of (er,y)cr2si2 compounds at ultra-low temperatures, Sci. China Mater. 66 (2023) 2039.
- [11] S. Mellari, Introduction to magnetic refrigeration: magnetocaloric materials, Int. J. Air-Cond. Refrig. **31** (2023) 5.
- [12] N. Chau, P. Q. Niem, H. N. Nhat, N. H. Luong and N. D. Tho, Influence of cu substitution for mn on the structure, magnetic, magnetocaloric and magnetoresistance properties of la0.7sr0.3mno3 perovskites, Phys. B: Condens. Matter 327 (2003) 214.
- [13] Y. Essouda, H. T. Diep, M. Ellouze and E. Hlil, Magnetic properties of perovskites pr0.9sr0.1 mn0.93+mn0.14+o3: Monte carlo simulations and experiments, J. Magn. Magn. Mater. 588 (2023) 171485.
- [14] Y. Essouda, H. T. Diep and M. Ellouze, First-order phase transition in perovskites pr0.67sr0.33mno3 magneto-caloric properties effect of multi-spin interaction, J. Magn. Magn. Mater. 599 (2024) 172105.
- [15] Y. Essouda, H. T. Diep and M. Ellouze, *Phase transition and magneto-caloric properties of perovskites* pr0.55sr0.45mno3: Modeling versus experiments, Phys. A: Stat. Mech. Appl. 635 (2024) 129532.
- [16] T.-L. Phan, Q. Tran, P. Thanh, P. Yen, T. Thanh and S. Yu, *Critical behavior of la0.7ca0.3mn1-xnixo3 manganites* exhibiting the crossover of first- and second-order phase transitions, Solid State Commun. **184** (2014) 40.
- [17] T. L. Phan, T. D. Thanh, T. A. Ho, T. V. Manh, Q. T. Tran, P. Lampen et al., An effective route to control the magnetic-phase transition and magnetocaloric effect of la0.7ca0.3mno3 nanoparticles, IEEE Trans. Magn. 50 (2014) 1.
- [18] M. Phan, V. Franco, N. Bingham, H. Srikanth, N. Hur and S. Yu, *Tricritical point and critical exponents of la0.7ca0.3-xsrxmno3* (x=0, 0.05, 0.1, 0.2, 0.25) single crystals, J. Alloys Compd. **508** (2010) 238.
- [19] J. Mira, J. Rivas, F. Rivadulla, C. Vazquez-Vazquez and M. A. Lopez-Quintela, Change from first- to second-order magnetic phase transition in la2/3(ca,sr)1/3mno3 perovskites, Phys. Rev. B 60 (1999) 2998.
- [20] T.-L. Phan, P. Zhang, Y. D. Zhang, D. Grinting, T. D. Thanh and S. C. Yu, Rounding of a first-order magnetic phase transition in la0.7ca0.3mn0.85ni0.15o3, J. Appl. Phys. 113 (2013) 17E150.
- [21] M. Blume, Theory of the first-order magnetic phase change in uo2, Phys. Rev. 141 (1966) 517.
- [22] H. Capel, On the possibility of first-order phase transitions in ising systems of triplet ions with zero-field splitting, Physica 32 (1966) 966.

- [23] I. Puha and H. Diep, Random-bond and random-anisotropy effects in the phase diagram of the blume-capel model, J. Magn. Magn. Mater. **224** (2001) 85.
- [24] E. Bezerra, M. G. da Silva and J. R. de Sousa, First-order transition of the spin-1 blume-capel model with random anisotropy using effective-field theory, Physica A 615 (2023) 128510.
- [25] P. H. Nguyen, N. T. Nguyen, H. D. Nguyen, H. T. Nguyen, C. T. Bach and G. H. Bach, Random-anisotropy driven giant magnetic entropy change in first-order magnetic transition under external fields, J. Alloys Compd. 1017 (2025) 179001.
- [26] O. K. Nguyen, P. H. Nguyen, L. D. Dang, C. T. Bach and G. H. Bach, Fluctuation inducing fractional magnetization behavior on the shastry–sutherland lattice, Phys. B: Condens. Matter 583 (2020) 412012.
- [27] P. H. Nguyen, Q. M. Le, O. K. Nguyen, C. T. Bach and G. H. Bach, Effective field theory investigation for a disordered ising model in the description of amorphous magnetic systems, J. Non-Cryst. Solids 643 (2024) 123165.
- [28] G. H. Bach, P. H. Nguyen, Q. D. Nguyen and S. N. Bui, Random-anisotropy effects in the second-order phase transition of the 2d blume-capel model, Comm. Phys. 35 (2025).
- [29] J. A. Plascak, A. M. Ferrenberg and D. P. Landau, *Cluster hybrid monte carlo simulation algorithms*, Phys. Rev. E **65** (2002) 066702.
- [30] N. Metropolis, A. W. Rosenbluth, M. N. Rosenbluth, A. H. Teller and E. Teller, Equation of state calculations by fast computing machines, J. Chem. Phys. 21 (1953) 1087.
- [31] U. Wolff, Collective monte carlo updating for spin systems, Phys. Rev. Lett. 62 (1989) 361.
- [32] K. Hukushima and K. Nemoto, Exchange monte carlo method and application to spin glass simulations, J. Phys. Soc. Jpn. 65 (1996) 1604.
- [33] O. K. T. Nguyen, P. H. Nguyen, N. T. Nguyen, C. T. Bach, H. D. Nguyen and G. H. Bach, Monte carlo investigation for an ising model with competitive magnetic interactions in the dominant ferromagnetic-interaction regime, Comm. Phys. 33 (2023) 205.
- [34] K. Binder, Finite size scaling analysis of ising model critical properties, Rep. Prog. Phys. 50 (1987) 783.
- [35] D. P. Landau and K. Binder, A Guide to Monte Carlo Simulations in Statistical Physics. Cambridge University Press, Cambridge, UK, 3rd ed., 2009.